



Removal of phenol by lignin-based activated carbon as an efficient adsorbent for adsorption of phenolic wastewater

Mengping Li¹ · Jincheng Mu² · Yanxiu Liu¹ · Huan Wang¹ · Yuanyuan Wang¹ · Hua Song¹

Received: 22 September 2022 / Accepted: 10 January 2023 / Published online: 7 February 2023
© The Author(s), under exclusive licence to Springer Nature B.V. 2023

Abstract

The different lignin-based biomass activated carbons were prepared by KOH activation from three different lignin sources [corn straw lignin (CSLAC), lignosulfonate lignin (LSAC) and bagasse lignin (BLAC)]. And the effects of different lignin sources, activation temperatures and adsorption conditions (adsorbent dosage, adsorption temperature and pH value) on the removal of phenol were systematically investigated. The results showed that different lignin-based biomass activated carbons, the CSLAC-based activated carbon exhibited the highest specific surface area and phenol adsorption capacity. And the CSLAC-*T* prepared at 800 °C (CSLAC-800) possessed specific surface area of 1679 m²/g, and the adsorption capacity of phenol reached 612 mg/g. The phenol removal rate of CSLAC-*T* was positively correlated with the specific surface area, and the adsorption rate of CSLAC-*T* was significantly higher than that before modification. In addition, the kinetic model, isothermal adsorption model and thermodynamic parameters of the three adsorbents were discussed. The results show that the three lignin-based activated carbons had a large adsorption capacity for phenol, which was spontaneous and exothermic adsorption. The adsorption is mainly through the π - π and hydrogen bond interactions, and hydrophobic effect.

Keywords Lignin · Activated carbon · Phenol · Wastewater treatment

✉ Jincheng Mu
jincheng292025@163.com

✉ Hua Song
songhua2004@sina.com

¹ Provincial Key Laboratory of Oil and Gas Chemical Technology, College of Chemistry and Chemical Engineering, Northeast Petroleum University, Daqing 163318, Heilongjiang, China

² Engineering Laboratory of Chemical Resources Utilization in South Xinjiang of XPCC, Tarim University, Xinjiang 843300, Alar, China

Introduction

Phenol and its derivatives are important chemical production raw materials and products, which are widely used in various industries such as petrochemical, coal chemical, pharmaceutical, dye and phenolic resin [1]. Phenolic compounds are one of the highly toxic organic pollutants. Low concentrations of phenol can denature proteins, while high concentrations can precipitate proteins, resulting in cell poisoning, damage to human skin and respiratory tract, and even nerve center paralysis [2, 3]. In addition, phenols also do great harm to aquatic organisms and crops. When the concentration of phenols in water exceeds 10 mg/L, organisms in water will die. Phenolic compounds have stable properties, wide sources, high toxicity, poor biodegradability and are difficult to be degraded in nature. Therefore, they are listed as one of the key pollutants to be controlled [4, 5]. How to effectively deal with phenolic pollutants is an urgent problem in the environmental field.

At present, there are many degradation methods of phenolic wastewater, including photocatalytic method [6], chemical oxidation method [7], electrochemical method [8], biological method [9], adsorption method [10], etc. Adsorption method is widely used in the treatment of phenolic wastewater due to its advantages of good removal effect, fast speed, low energy consumption, diverse adsorption materials, etc. [11]. Common adsorbents include activated carbon, resin, graphene, molecular sieve, metal organic framework, etc. [12–15]. With the continuous improvement of the performance of existing adsorbents and the research and development of new adsorbents, the adsorption method has a good application prospect and market value in the treatment of phenol containing wastewater.

Activated carbon has porous structure, high specific surface area, developed pore structure, rich functional groups on its surface, strong adsorption capacity, stable chemical properties, good acid and alkali resistance, good heat resistance and high mechanical strength. At present, there are many researches on the preparation of activated carbon from biomass wastes, such as straw, fruit shell, coal and sawdust [16–18]. Franco et al. [19] used the fruit waste of kapok tree as raw material to prepare activated carbon for removing phenol from water. The specific surface area of activated carbon was 842 m²/g. The thermodynamic results show that the adsorption of phenol is spontaneous and exothermic. Song et al. [20] Prepared high-efficiency activated carbon (AC_{psr}) from peony seed shell residue (PSR). AC_{psr} was systematically characterized, and the adsorption performance of AC_{psr} for phenol was optimized by response surface methodology (RSM), and its adsorption mechanism was studied. The results show that AC_{psr} has a high specific surface area of 1499.5 m²/g and highly developed pore structure. The optimal adsorption efficiency of AC_{psr} was 93.11%. AC_{psr} can effectively remove phenolic pollutants in solution. As an economical and environment-friendly biomass precursor, biomass waste residue has great potential in remediation of water pollution.

There have been a lot of studies on the preparation of activated carbon from biomass waste for adsorption of phenolic wastewater. Biomass contains cellulose, hemicellulose and lignin. Cellulose and hemicellulose can be used to ferment cellulosic ethanol or paper making. Lignin is one of the three major components

of biomass, in the pulp and paper industry and bio-fermentation to produce fuel ethanol and other industries, due to the complex structure and stable nature of lignin, it is difficult to be used and degraded. The lignin is usually separated and removed by various methods, and the lignin component is discharged from the system as residual waste. The industrial lignin produced every year in the world is very huge, up to 150–180 million tons, only about 2% of lignin has been used, most of the remaining lignin has not been effectively used, but is directly discharged into the environment or burned as low-value fuel [21–23], which not only wastes resources, but also causes serious pollution to the environment. With the shortage of non-renewable fossil resources and strict environmental protection requirements, the efficient and high-value utilization of lignin has become a research focus. Solange et al. [24] used H_3PO_4 to chemically activate lignin from brewer's spent grain (BSG) to prepare different types of activated carbon with different acid/lignin ratios and different carbonization temperatures. The results showed that the BET surface area of BSG lignin carbon was between 33 and 692 m^2/g , and BSG lignin carbon showed high adsorption capacity for metal ions (mainly nickel, iron, chromium and silicon), and also reduced the concentration of phenolic compounds. These results indicate that BSG lignin can be used to prepare activated carbon with similar characteristics and high adsorption capacity as commercial activated carbon. Fu et al. [25] obtained black liquor lignin from the pulp and paper industry as a precursor to prepare activated carbon by steam physical activation. The effects of carbonization temperature, activation temperature and activation time on the pore structure of the product were investigated. The results showed that under the optimum preparation conditions, lignin-based activated carbon (LAC) was used to adsorb and remove methylene blue (MB) from aqueous solution, with the maximum adsorption capacity of 92.51 mg/g . The results show that LAC has great potential for dye wastewater treatment.

Lignin is always presented in the form of waste in the three components of biomass, which has not been fully utilized. In this study, corn straw lignin, lignosulfonate and bagasse lignin are selected as three industrial representative lignin raw materials, because they are generally derived from the pulping process of paper industry and the fermentation of ethanol industry and alcohol industry by lignin biomass. As industrial by-products and industrial waste residues, most of lignin are directly burned as biofuels, with low utilization rate and certain pollution to the environment. However, there are few reports on the use of lignin as the raw material for the preparation of activated carbon for the treatment of phenol containing wastewater. In this way, lignin can be utilized with high added value, and the waste of resources and pollution caused by waste treatment can be reduced. KOH activation method is the most effective method to prepare lignin-based activated carbon with high specific surface area [26]. In this paper, KOH activation method is used to prepare lignin-based activated carbon, which expands the raw material source of activated carbon, finds a new application field for a large number of low-efficiency utilization of lignin, and realizes the efficient resource utilization of lignin. This paper selects industrial lignin from different sources. On the one hand, it proves the feasibility and universal applicability of lignin as raw material for preparing activated carbon; on the other hand, it explores the differences in yield and adsorption

performance of different kinds of lignin for preparing activated carbon, providing basis for rational utilization of these resources.

Experimental

Materials

Corn straw lignin (CSL), lignosulfonate (LS, produced in Jiangsu), bagasse lignin (BL, produced in Guangxi), potassium hydroxide (Tianjin DaMao Chemical plant, analytical purity), high-temperature tubular furnace (ZY-1400), ultraviolet visible spectrophotometer (TU-1901), phenol (Tianjin DaMao Chemical plant, analytical purity).

Preparation of activated carbon

A certain amount of corn straw lignin (CSL) was washed repeatedly with distilled water to remove the inorganic salt impurities, and then soaked in distilled water at 80 °C for 8 h and suction filtration. The obtained solid was dried at 105 °C for 24 h, which was recorded as CSLAC. A certain amount of pretreated CSLAC was mixed with potassium hydroxide (mass ratio: 1:1), soaked in distilled water for 3 h, and filtered solid was dried at 120 °C for 24 h. The obtained solid was placed in a tubular furnace under nitrogen atmosphere, and the temperature was raised from room temperature to 250 °C at a heating rate of 3 °C/min for 2 h, and then, the temperature was raised to the required activation temperature ($T=600, 700, 800, 900$) at a heating rate of 3 °C/min for 3 h. The lignin activated carbon obtained is recorded as CSLAC- T , and T is the activation temperature.

With the above method, lignosulfonate (LS) and bagasse lignin (BL) were treated with other conditions unchanged, and the activation temperature was fixed at 800 °C. The solids obtained were recorded as LSAC-800 and BLAC-800, respectively.

Structural characterization

The Brunauer–Emmett–Teller (BET) method was used to measure the specific surface area, and the classic Barrett–Joyner–Halenda (BJH) model was used to calculate the pore size distribution. The samples were characterized by X-ray diffraction (XRD) and recorded on a (Philips X'Pert-Pro-Super) X-ray powder diffractometer with Cu-K α radiation. Under the setting conditions of 40kV and 30 mA, the scanning range was 0.5°–10°, and the rate is 1/6° min⁻¹. Functional groups are examined by Fourier transform infrared spectroscopy (FT-IR) (Bruker company was used for determination). The sample characterization method is to grind the dried activated carbon sample to be tested together with KBr into powder and press it into pieces. The scanning range was 4000–400 cm⁻¹, the samples were detected, and the functional groups on the surface of activated carbon were qualitatively analyzed. Under vacuum conditions with an acceleration voltage of 100 V–30 kV, a scanning electron microscope (SEM) was obtained

on the SIGMA scanning electron microscope from Carl Zeiss AG, Germany, and the sample was magnified to 2000–10,000 times.

Determination of pH point of zero charges (pH_{pzc})

Taking corn straw lignin activated carbon as an example, 5.0 mg CSLAC-800 was added to five beakers containing 25 mL KCl solution (0.1 mol/L), and the initial pH (pH_0) was adjusted to 5.0, 6.0, 7.0, 8.0 and 9.0, respectively. After stirring for 10 min, the suspension was placed in room temperature air for 24 h. Solid was then removed from the suspension by centrifugation, and the final pH (pH_e) of the liquid was measured with a pH meter. The plot of ΔpH ($\Delta\text{pH} = \text{pH}_0 - \text{pH}_e$) to pH_0 was drawn, and pH_{pzc} is calculated at $\Delta\text{pH} = 0$.

Adsorption experiments

Each time, 20 mL of phenol solution (150 mg/L) was put into a small brown bottle, 0.015 g adsorbent was added, and the small brown bottle was placed on the magnetic stirrer at a rate of 300 r/min. The adsorption was carried out at 30 °C for 2 h. After the adsorption reached equilibrium, the supernatant was extracted with a syringe and filtered through a 0.2 μm syringe membrane filter. The absorbance value of the filtered solution was measured, and the measured absorbance value was substituted into the standard curve to obtain the concentration of phenol (See Fig. S1 for standard curve). The adsorption capacity and adsorption rate were used as the evaluation indexes of phenol adsorption effect, the adsorption rate and adsorption capacity are calculated according to Eqs. (1) and (2), respectively.

$$\text{AR}(\%) = \frac{C_0 - C_e}{C_0} \times 100\% \quad (1)$$

where C_0 is the initial concentration of phenol solution (mg/L), C_e is the concentration when the phenol solution reaches the adsorption equilibrium (mg/L), and AR is the adsorption rate (%) when the adsorption process reaches the adsorption equilibrium.

$$Q_e = \frac{V}{m_c}(C_0 - C_e) \quad (2)$$

where Q_e represents the adsorption capacity (mg/g) when the adsorption equilibrium is reached, V represents the volume of phenol solution (L) without adsorption, and m_c represents the amount of adsorbent added in each group of adsorption experiments (g).

Experimental data models

Pseudo-first-order kinetic models and pseudo-second-order kinetic models are the most commonly used kinetic models for adsorption. The pseudo-first-order kinetic model is shown in Eq. 3.

$$Q_t = Q_e(1 - e^{-k_1 t}) \quad (3)$$

where t represents the adsorption time, Q_t represents the adsorption capacity (mg/g) of the adsorbent at time t (min), Q_e represents the adsorption capacity (mg/g) when the adsorption process reaches the adsorption equilibrium, and k_1 represents the adsorption rate constant (min^{-1}).

While the pseudo-second-order kinetics model is shown in Eq. 4, [27, 28]

$$Q_t = \frac{k_2 Q_e^2 t}{1 + k_2 Q_e t} \quad (4)$$

where k_2 represents the adsorption rate constant, (g/mg min).

The Langmuir isothermal model (Eq. 5) and Freundlich isothermal model (Eq. 6) are shown as:

$$Q_e = \frac{Q_{\max} K_L C_e}{1 + K_L C_e} \quad (5)$$

$$Q_e = K_F C_e^{1/n} \quad (6)$$

where Q_{\max} represents the maximum adsorption capacity (mg/g) of the adsorbent when the monolayer adsorption reaches saturation, Q_e represents the adsorption capacity (mg/g) at adsorption equilibrium, and K_L represents the Langmuir constant related to the adsorption energy (L/mg). K_F represents the Freundlich isotherm constant ($\text{mg/g}(\text{L/mg})^{1/n}$), and $1/n$ indicates the effect of solution concentration on adsorption capacity. If $1/n$ is between 0.1 and 0.5, adsorption is easy, and if $1/n$ is greater than 2, adsorption is difficult [29–32].

Results and discussion

Characterization of the AC samples

TGA analysis

The TGA curves of solid samples of corn straw lignin (CSL), lignosulfonate (LS) and bagasse lignin (BL) under nitrogen atmosphere are shown in Fig. S2. It can be seen from Fig. S2 that the pyrolysis process of lignin was mainly divided into three weight-loss stages. The first weight-loss stage was below 200 °C, and the mass loss

in this stage was the free water evaporation of the material, namely the drying and dehydration stage [33]. At this stage, the mass loss of CSL, LS and BL was 5.9%, 4.9% and 1.8%, respectively. The second weight-loss stage is between 200 °C and 600 °C, which is one of the main stages of lignin pyrolysis. The mass loss in this stage is the removal of small and medium-sized volatile components of lignin. In this stage, the aliphatic hydroxyl functional groups in the branch chain structure of lignin break into small molecules of water, and the C–C bond and ether bond in lignin break, producing a series of small molecules such as CO, CO₂ and CH₄ volatilization. The carbon skeleton is basically generated in this stage [34]. At this stage, the mass loss of corn straw lignin, liginosulfonate and bagasse lignin was 36.4%, 35.8% and 28.9%, respectively. The third weight-loss stage is above 600 °C. In this stage, lignin aromatic ring structure and aryl ether bonds are decomposed at high temperature to produce various phenolic substances and a large amount of CO and CO₂, and the carbon skeleton is further consumed and pyrolyzed [35–37]. The mass loss of corn straw lignin, liginosulfonate and bagasse lignin in this range is about 5.8%, 9.7% and 9.2%, respectively, and the weight loss is relatively slow. As can be seen from Fig.S2, the decomposition of the three kinds of lignin has been basically completed at 600 °C, and with a small amount of mass loss, the structure of carbon has basically been formed. The pyrolysis residue rates of CAL, LS and BL were 52.3%, 52.8% and 57.1%, respectively.

N₂ adsorption–desorption

The N₂ adsorption–desorption isotherm plots provide important information regarding the porosity of the carbon samples (Fig. 1; Table 1). From Fig. 1a, it can be seen that the shape of CSLAC and CSLAC-*T* adsorption isotherms is similar, belonging to Type IV [38]. When the relative pressure P/P_0 is less than 0.2, the adsorption capacity of activated carbon increases rapidly with the increase in relative pressure, and the adsorption rate is fast. This is due to the rapid filling of micropores in this pressure stage, which indicates that there are micropores in the prepared activated carbon [39]. When the relative pressure P/P_0 is greater than 0.2, the adsorption capacity continues to increase with the increase in the relative pressure, but the upward trend slows down. Due to the multi-molecular layer adsorption of gas molecules in the mesopores and macropores of activated carbon, the adsorption rate decreases, indicating that there is a certain amount of mesopores in activated carbon. When the relative pressure is greater than 0.9 and close to 1, the adsorption rate increases, because the adsorption of nitrogen molecules occurs in macropores, indicating that there are a certain amount of macropores in activated carbon. When the relative pressure P/P_0 is greater than 0.4 and less than 1, there is an obvious hysteresis loop. The adsorption isotherm and desorption isotherm do not coincide, and there is an obvious hysteresis loop, which is caused by capillary condensation in the mesopores, indicating that lignin-based activated carbon contains a large number of mesopores [40]. Therefore, the prepared CSLAC and CSLAC-*T* contains a large number of micropores and mesopores. In the whole range of nitrogen adsorption and desorption pressure, the nitrogen adsorption capacity increases gradually with the increase in activation temperature from 600 to 800 °C, the micropore and

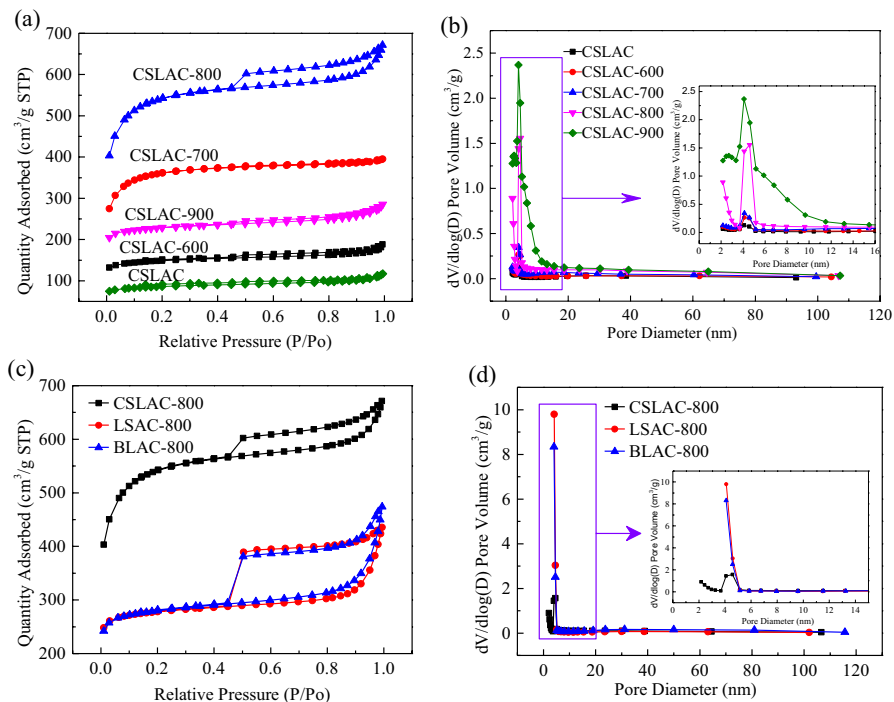


Fig. 1 Adsorption isotherm curve (a) and pore size distribution curve (b) of CSLAC and CSLAC-*T*; Adsorption isotherms (c) and pore size distribution curves (d) of CSLAC-800, LSAC-800 and BLAC-800

Table 1 Pore structure and yield of lignin-based activated carbon

Sample	S_{BET} ($\text{m}^2 \text{g}^{-1}$)	Pore diameter (nm)	Pore volume ($\text{cm}^3 \text{g}^{-1}$)	Micropore area ($\text{m}^2 \text{g}^{-1}$)	Mesopore area ($\text{m}^2 \text{g}^{-1}$)	Yield (%)
CSLAC	265	6.20	0.071	206	59	45.4
CSLAC-600	454	5.98	0.092	371	83	43.5
CSLAC-700	1114	3.33	0.138	755	359	32.0
CSLAC-800	1679	4.86	0.369	1079	600	26.8
CSLAC-900	695	6.44	0.128	590	105	3.30
CSLAC-800	1679	4.86	0.369	1079	600	26.8
LSAC-800	844	12.43	0.294	718	126	44.1
BLAC-800	856	12.19	0.364	697	159	46.5

mesopore structures are rich, and the pore capacity increases. After the activation temperature reaches above 800 °C, continue to increase the activation temperature, when the activation temperature reaches 900 °C, the nitrogen adsorption capacity, microporous and mesoporous structures and pore capacity decrease [41, 42]. It can be seen from Figure (b) that for CSLAC-*T* (600–800 °C), the most probable

mesopores of the material are around 4–5 nm, while mesopores larger than 5 nm appear in CSLAC-900, which may be the reason for the obvious reduction of pore volume.

It can be seen from Table 1 that compared with CSLAC, the specific surface of CSLAC-*T* activated at different temperatures was increased, indicating that KOH activation could significantly increase lignin specific surface area. When the activation temperature rises from 600 to 800 °C, the specific surface area of the prepared activated carbon gradually increases from 454 to 1679 m²/g, the pore capacity gradually increases, and the pore diameter decreases. When the activation temperature continues rises from 800 to 900 °C, the specific surface area decreases to 695 m²/g, and the pore volume decreases with the pore diameter increases. This is because when the temperature is low, the water in lignin is evaporated and released to form micropores. With the increase in temperature, the branched aliphatic hydroxyl and carboxyl functional groups in lignin are pyrolyzed to produce water molecules, and small molecules such as CO and CO₂ are volatilized from the system to produce a large number of micropores, resulting in the increase in the specific surface area of the material. When the temperature rises to 500–600 °C, KOH reacts with the carbon side chain in lignin and the carbon in the skeleton, generate large amounts of hydrogen, produce new microporous while the micropores generated at the initial stage of pyrolysis expanding to form larger micropores and mesopores. At this stage, the pores are mainly micropores, with the total specific surface area increasing, the pore volume increasing and the average pore size decreasing. As the temperature continues to rise to 800 °C, the activator reacts with the carbon chain to generate volatile substances such as hydrogen, CO, CO₂ and CH₄, and the micropores are fully developed to form a large number of mesopores, Moreover, when the temperature is higher than 773 °C, the simple substance of metal potassium evaporates. During the evaporation process, it will enter the carbon interlayer, open the carbon layer to produce new micropores, and the pore structure is rich. At this stage, the pore structure is mainly mesoporous, so the specific surface area and pore volume of activated carbon increase, and the average pore size increases. When the temperature continues to rise to 900 °C, the reaction rate between KOH and carbon is too fast, and the evaporation rate of metal potassium increases too fast, as a result, the micropores of activated carbon are ablated into mesopores or even macropores, and the macropores continue to be burned and expanded, resulting in the destruction of the pore structure. At the same time, the pore wall between adjacent pores is broken due to high-temperature burning, resulting in the collapse of the pore structure. Therefore, too high a temperature will lead to the destruction of the pore structure, the reduction of the specific surface area and the increase in the average pore diameter, which are consistent with the results of the pore size distribution map [43, 44].

It can be seen from Fig. 1c that the adsorption isotherms of LSAC-800 and BLAC-800 are similar to those of CSLAC-800, but the nitrogen adsorption capacity of corn stover lignin-based activated carbon CSLAC-800 is the largest in the whole pressure range, with rich microporous and mesoporous structures and large pore capacity. It can be seen from Table 1 that the specific surface area and pore capacity of CSLAC-800 corn stalk lignin are the largest among the activated carbons obtained from three different lignin activated with KOH at 800 °C. The pore

size distribution can be seen from Fig. 1d that the three kinds of lignin-based activated carbon are mainly mesoporous, containing a certain amount of micropores and macropores, and the pore structure is developed.

Table 1 lists the effect of different activation temperatures on the yield of activated carbon. With the increase in temperature, the yield of activated carbon gradually decreases. When the temperature rises to 900 °C, the yield of activated carbon is only 3.3%. This is because with the increase in temperature, the more intense the reaction between activator and carbon, the greater the loss of carbon in lignin, and the lower the yield of activated carbon. Among the three kinds of lignin-based activated carbon, the yield of corn straw lignin-based activated carbon CSLAC-800 is the lowest, the yield of bagasse lignin activated carbon BLAC-800 is the highest.

SEM analysis

Figure 2 is the SEM diagram of samples before and after modification. From Fig. 2 a, c, e, it can be seen that the morphology of the original three kinds of lignin is much different. Before unmodified and activated, the lignin of corn straw presents a rod-like fiber structure, the lignosulfonate presents a multi fold and large block structure, and the bagasse lignin presents a small fragment structure. It can be seen from Fig. 2b, d, f that after KOH activation and modification, all sample surfaces have pores of different sizes, and the pore structure is developed. This is due to the pore-forming effect of KOH in the high-temperature activation process, which can endow the adsorbent with rich pores. Among them, CSLAC-800 has the most abundant pore structure, which is conducive to increasing its specific surface area, which is consistent with the BET analysis. However, the surface of BLAC-800 (Fig. 2f) has formed large pores. The rich pore structure and large specific surface area are conducive to improving the adsorption capacity of phenol [45]. See supplementary material S1–S5 for the detailed mechanism of KOH activation and pyrolysis of biomass.

FT-IR analysis

The functional groups on the surface of activated carbon are one of the important factors affecting the adsorption performance of activated carbon. Figure 3 shows the FT-IR diagram of samples before and after modification, as shown in Fig. 3a, CSLAC has a wide peak at about 3424 cm^{-1} , which is the stretching vibration characteristic peak of alcohol hydroxyl or phenolic hydroxyl. There is a smaller peak about 2915 cm^{-1} , which includes the stretching vibration characteristic peaks of $-\text{CH}_3$, $-\text{CH}_2$, $-\text{CH}$ and methoxy C–H in aromatic ring. The absorption peaks at 1664 cm^{-1} included C=O characteristic peaks of carboxyl group, ester group and ketone. The characteristic peak around 1510 cm^{-1} is related to the C=C stretching vibration of the aromatic ring skeleton. The characteristic peak around 1449 cm^{-1} is related to the symmetric stretching vibration of $-\text{C}=\text{O}$, and the absorption peak around 1103 cm^{-1} , 1042 cm^{-1} is the characteristic peak of ether bond and CO of ester group. In contrast to CSLAC, the functional groups of CSLAC-*T* are basically the same. The hydroxyl absorption

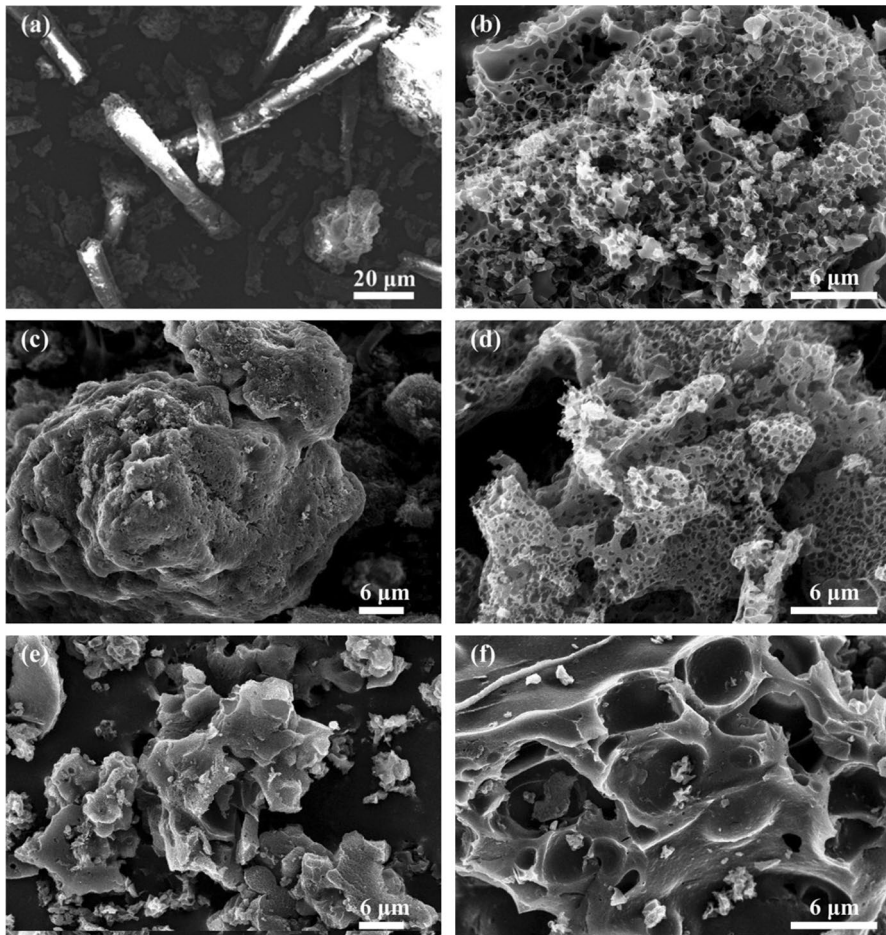


Fig. 2 SEM images of CSL unmodified activation (a), LS unmodified activation (c), BL unmodified activation (e), CSLAC-800 (b), LSAC-800 (d), BLAC-800 (f)

peak appeared at 3424 cm^{-1} , the carboxyl group appeared at 1660 cm^{-1} , the $\text{C}=\text{O}$ characteristic peak of ester group appeared at 1449 cm^{-1} , the $\text{C}=\text{C}$ stretching vibration peak of aromatic ring skeleton appeared at 1510 cm^{-1} and the $\text{C}-\text{O}-\text{C}$ stretching vibration characteristic peak appeared at 1042 cm^{-1} . It can be seen from the infrared spectrum that lignin contains hydroxyl, carboxyl, carbonyl, benzene ring, etc. After high-temperature activation, the types of functional groups are reduced [46–49].

It can be seen from the infrared spectrum in Fig. 3b that the three kinds of lignin contain basically the same types of functional groups, including hydroxyl, carboxyl, carbonyl, methoxy, benzene ring, etc. After high-temperature activation at $800\text{ }^{\circ}\text{C}$, the types of functional groups decrease.

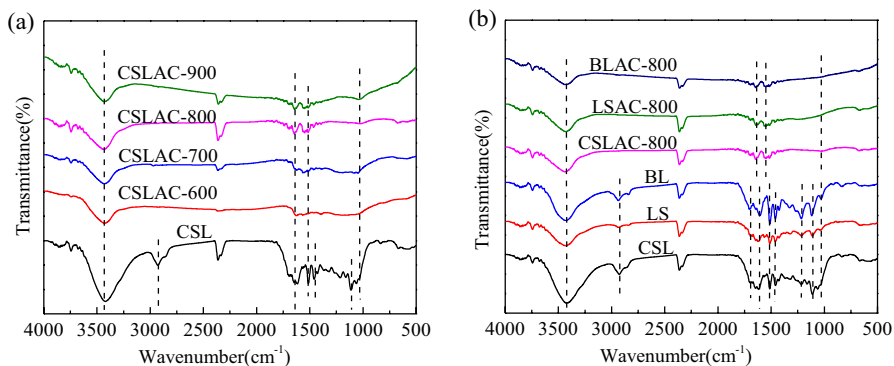


Fig. 3 Infrared spectrum of CSLAC and CSLAC-*T*, CSLAC-800 (a) and CSLAC-800, LSAC-800, BLAC-800 (b)

XRD analysis

The XRD analysis results of lignin-based activated carbon are shown in Fig. 4. It can be seen from Fig. 4 that all samples have a wide diffraction peak at $2\theta=20^{\circ}$ – 26° , which corresponds to the (002) crystal plane of amorphous carbon, while the diffraction peak at $2\theta=43^{\circ}$ is the (100) crystal plane of graphite carbon, indicating that the material contains amorphous carbon and graphite carbon. It can be seen from Fig. 4a that, with the increase in activation temperature, there is an obvious peak at $2\theta=43^{\circ}$ of CSLAC-*T*, indicating that the graphitization degree increases. At a lower activation temperature, there is an obvious peak at $2\theta=26^{\circ}$, indicating that the activated carbon activated at a lower temperature contains more mineral impurities. It can be seen from Fig. 4b that the graphitization degree of CSLAC-800 and LSAC-800 was higher in the activated carbons activated at 800 °C. Except for two characteristic peaks at (002) and (100), no other diffraction peaks are found in the spectrogram, indicating that the

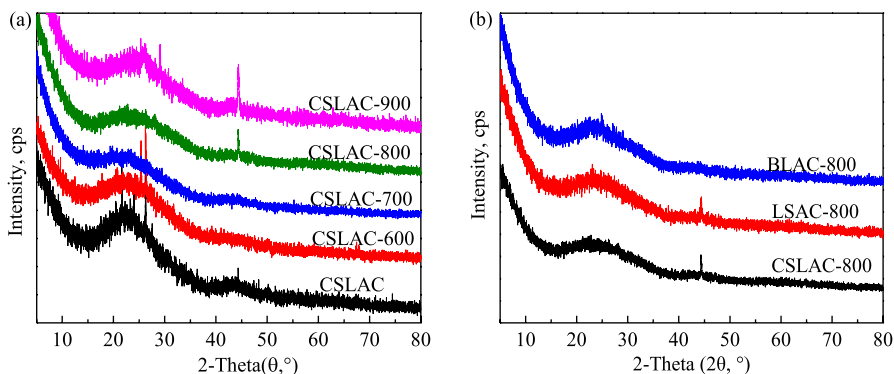


Fig. 4 XRD Spectra of CSLAC-*T* (a) and CSLAC-800, LSAC-800, BLAC-800 (b)

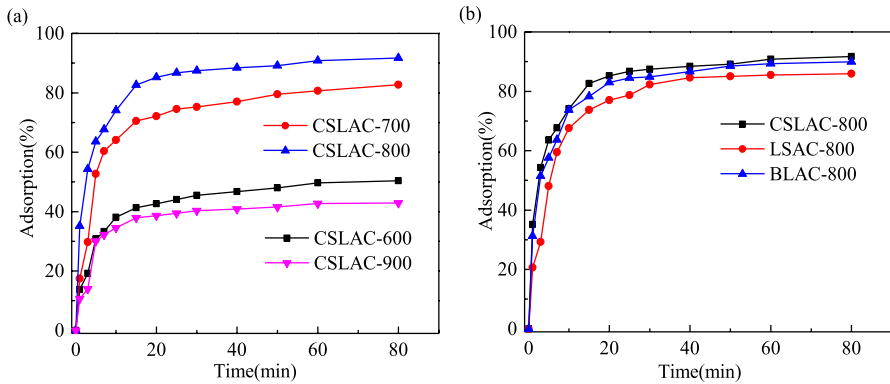
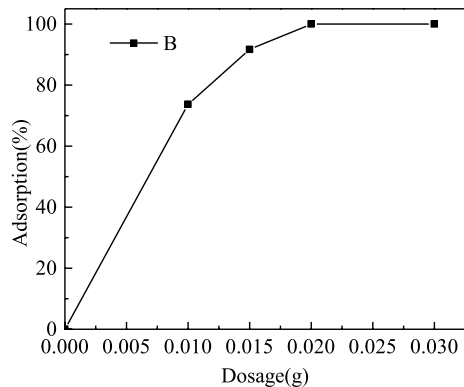


Fig. 5 Effect of activation temperature on phenol adsorption over CSLAC-*T* (a) and effect of different adsorbents on phenol adsorption (b) (adsorption conditions: $V=20$ mL, $C_0=150$ mg/L, $m_c=0.015$ g, $T=30$ °C and $t=80$ min)

Fig. 6 Effect of CSLAC-800 dosage on phenol adsorption (adsorption conditions: $V=20$ mL, $C_0=150$ mg/L, $T=30$ °C and $t=80$ min)



inorganic mineral impurities in the activated carbons activated at 800 °C have been removed [50–52].

Adsorption experiment

Effect of activation temperature and different lignin on phenol adsorption

Figure 5a shows the effect of activation temperature on the adsorption performance of CSLAC-*T* phenol (adsorption conditions: 20 mL phenol solution ($C_0=150$ mg/L), 0.015 g adsorbent, adsorption temperature 30 °C). It can be seen from Fig. 6 that the adsorption rate of all samples increases sharply at first, then slowly and finally tends to a stable value. After adsorption for 60 min, the adsorption basically reached equilibrium. As the activation temperature rises from 600 to 800 °C, the equilibrium adsorption rate of CSLAC-*T* for phenol gradually increases, but when the activation temperature continues to rise to 900 °C, the adsorption rate decreases, and the

adsorption rate of CSLAC-800 for phenol is the largest, reaching 91.7%. This may be due to the fact that CSLAC-800 has the highest specific surface area and pore volume (Table 1) and abundant pore structure. It was also found that the adsorption capacity of CSLAC-*T* for phenol was positively related to the specific surface area of activated carbon. It can be seen from Fig. 6b that among the activated carbons obtained by modifying and activating different lignin under the same conditions, the adsorption rate of phenol of corn straw lignin-based activated carbon CSLAC-800 is the highest and the best.

Effect of adsorbent amount on phenol adsorption

In order to determine the appropriate amount of adsorbent, other conditions unchanged (adsorption conditions: 20 mL phenol solution ($C_0 = 150$ mg/L), 0.015 g adsorbent, adsorption temperature 30 °C, adsorption time 80 min), the effect of the amount of CSLAC-800 on phenol adsorption was studied. As shown in Fig. 6, the adsorption rate of phenol gradually increased with the increase in adsorbent amount. When 0.02 g of CSLAC-800 was added, the adsorption rate of phenol reached 100%.

Determination of pH_{pzc} and effect of pH

The pH of the solution is an important parameter affecting the adsorption rate of phenolic compounds. The surface charge of adsorbent in solutions at different pH depends on its zero point of charge (pH_{pzc}). The pH_{pzc} value of adsorbent is the electrostatic characteristics of its surface. When the solution pH is greater than pH_{pzc} of the material, the surface of material is negatively charged, while when the solution pH is less than pH_{pzc} , the surface of material is positively charged. To study effect of pH on phenol removal over CSLAC-800, its pH_{pzc} was measured and the result is shown in Fig. 7a. As can be seen from Fig. 7a, the pH_{pzc} value of CSLAC-800 is 7.2. Therefore, if the pH of the solution is less than 7.2, the surface of CSLAC-800

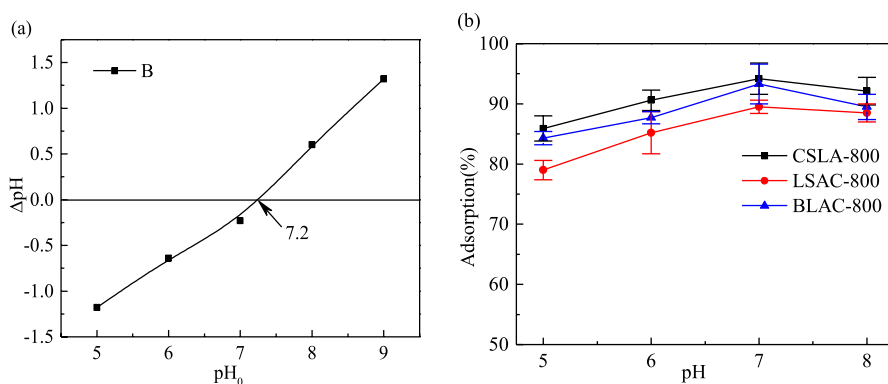


Fig. 7 pH_{pzc} curve of BAC-800 (a), effect of pH on phenol adsorption (b). (Adsorption conditions: $V = 20$ mL, $C_0 = 150$ mg/L, $m_c = 0.015$ g, $T = 30$ °C and $t = 80$ min)

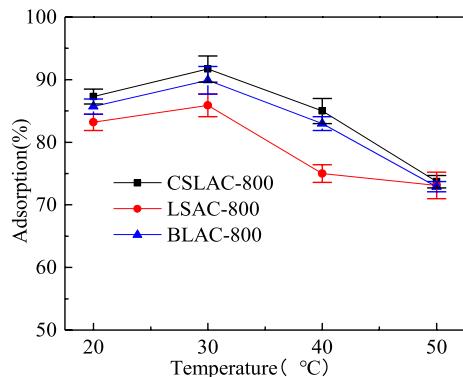
is positively charged. If the pH of the solution is greater than 7.2, the surface of the CSLAC-800 is negatively charged [53–56]. Furthermore, phenol solution is a weakly acidic solution with pK_a of 10.0. Therefore, the phenol molecules are ionized to form phenoxy negative ions in solution and high pH promotes the ionization of phenol [57].

Effect of pH (5–8) on phenol adsorption over three lignin-based activated carbons was studied with the other conditions remained unchanged. As shown in Fig. 7, the adsorption rate of the three lignin-based activated carbons gradually increases with the increase in pH value, until the adsorption rate reaches the maximum value when the pH value is 7.0, which are 94.2% for CSLAC-800, 89.5% for LSAC-800 and 93.3% for BLAC-800, respectively. This is because when pH of the solution is 7.0, the surface of adsorbent is positively charged owing to the pH is less than pH_{pzc} of adsorbent ($pH_{pzc} = 7.2$). And the phenol molecules are ionized to form phenoxy negative ions. The positively charged adsorbent surface attracts the phenoxy negative ions, leading to high phenol removal rate for $pH = 7$. However, with the decrease in pH value, ionization effect of phenol gets weak, therefore the phenol removal rate is decreased. Interestingly, the adsorption rate decreases with increase in pH when $pH > 8.0$ (Fig. 7). This is possibly because for $pH > 8.0$, the surface of adsorbent is negatively charged owing to pH is higher than its pH_{pzc} ($pH_{pzc} = 7.2$), which would electrostatically repulse the phenoxy negative ions. This leads to decrease in the adsorption rate with increase in pH for alkaline solution with $pH > 7.2$ because higher pH value promotes formation of cations.

Effect of adsorption temperature

The influence of adsorption temperature (20–50 °C) on the adsorption of phenol by CSLAC-800, LSAC-800 and BLAC-800 adsorbents is shown in Fig. 8. It can be seen from Fig. 8 that with the increase in adsorption temperature from 20 to 30 °C, the adsorption performance of the three kinds of lignin-based activated carbon for phenol improves, but with the increase in adsorption temperature from 30 to 50 °C, the adsorption capacity of phenol decreases gradually. When the adsorption temperature was 30 °C, the adsorption rates of the three kinds of lignin-based activated

Fig. 8 Effect of three different lignin-based activated carbons on phenol adsorption at different solution temperatures (adsorption conditions: $V = 20$ mL, $C_0 = 150$ mg/L, $m_c = 0.015$ g and $t = 80$ min)



carbon for phenol are the largest, which were 91.7% for CSLAC-800, 85.9% for LSAC-800 and 89.9% for BLAC-800, respectively. The experiment shows that the adsorption temperature of 30 °C was the best adsorption temperature of adsorbent, so the adsorption temperature of 30 °C was selected in this experiment. It can also be seen from Fig. 8 that under different temperatures, the adsorption performance of CSLAC-800 for phenol is the best.

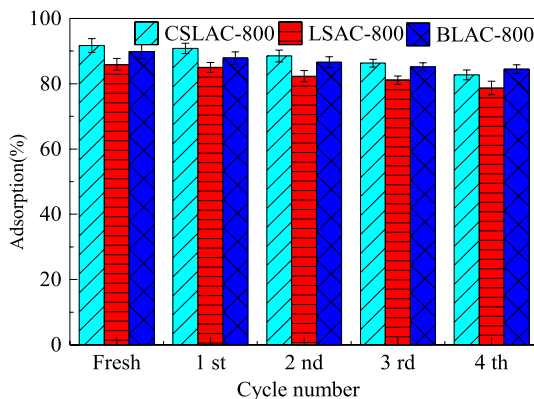
Recycling performance of adsorbent

In order to study the regeneration performance of the prepared adsorbents, the used adsorbent was soaked in methanol for 2 h, dried at 80 °C for 8 h and used for the next adsorption, the results are shown in Fig. 9. It can be seen from Fig. 9 that after four cycles, the adsorption rates of the three kinds of lignin-based activated carbon CSLAC-800, LSAC-800 and BLAC-800 have decreased (78.7–84.5%). Among them, CSLAC-800 had the best regeneration performance. After four cycles, it could still maintain the adsorption capacity of 84.5%, showing good adsorption performance.

Adsorption kinetics

The experimental data are fitted with pseudo-first-order and pseudo-second-order kinetic models, respectively, and the results are shown in Fig. 10 and Table 2. According to the results shown in Table 2, the correlation coefficient R^2 of CSLAC-800 pseudo-first-order kinetic model is 0.9507, the equilibrium adsorption capacity is 169.3 mg/g, and the actual experimental result is 180.2 mg/g. For the pseudo-second-order model, the correlation coefficient R^2 is 0.9939, and the equilibrium adsorption capacity is 181.8 mg/g. Compared with the pseudo-first-order kinetic model, the pseudo-second-order kinetic model is closer to the experimental value and has higher correlation. Therefore, the pseudo-second-order model is more suitable to describe the adsorption kinetics of phenol on CSLAC-800. The correlation coefficient R^2 of LSAC-800 pseudo-first-order kinetic model is 0.9800, the

Fig. 9 Regeneration performance of adsorbent CSLAC-800, LSAC-800 and BLAC-800 (adsorption conditions: $V=20$ mL, $C_0=150$ mg/L, $m_c=0.015$ g, $T=30$ °C and $t=80$ min)



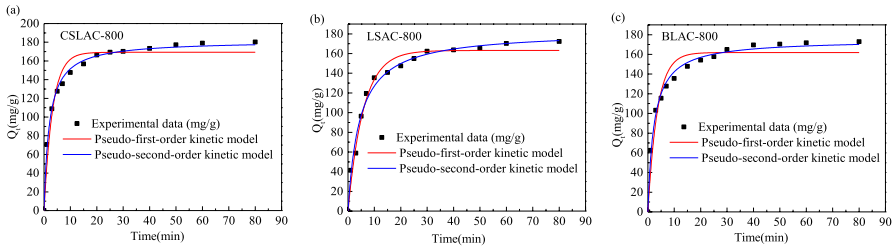


Fig. 10 Dynamic model fitting curve of CSLAC-800 (a), LSAC-800 (b) and BLAC-800 (c)

Table 2 Fitting results of adsorption kinetics of CSLAC-800, LSAC-800 and BLAC-800 adsorbents

Kinetic model	Parameters	CSLAC-800	LSAC-800	BLAC-800
Pseudo-first-order kinetic model $Q_t = Q_e(1 - e^{-k_1 t})$	$Q_{e,exp}$ (mg/g)	180.2	172.2	172.9
	$Q_{e,cal}$ (mg/g)	169.5	163.2	161.9
	K_1 (min^{-1})	0.3113	0.1714	0.2787
	R^2	0.9507	0.98	0.9437
Pseudo-second-order kinetic model $Q_t = \frac{k_2 Q_e^2 t}{1 + k_2 Q_e t}$	$Q_{e,cal}$ (mg/g)	181.8	182.7	175.0
	K_2 (min^{-1})	0.0028	0.0013	0.0026
	R^2	0.9939	0.9877	0.9909

equilibrium adsorption capacity is 163.2 mg/g, and the actual experimental result is 172.2 mg/g. For the pseudo-second-order model, the correlation coefficient R^2 is 0.9877, and the equilibrium adsorption capacity is 182.7 mg/g. The experiment shows that both the pseudo-first-order kinetic model and the pseudo-second-order kinetic model can describe the adsorption kinetics of phenol on LSAC-800. The correlation coefficient of BLAC-800 pseudo-first-order kinetic model is $R^2 = 0.9437$, the equilibrium adsorption capacity is 161.9 mg/g, the correlation coefficient of pseudo-second-order kinetic model is $R^2 = 0.9909$, the equilibrium adsorption capacity is 175.0 mg/g, and the actual adsorption capacity of the experiment is 172.9 mg/g. Compared with the first-order kinetics, the pseudo-second-order kinetics is close to the experimental value, and the correlation is higher. Therefore, the pseudo-second-order kinetic model is more suitable to describe the adsorption kinetics of phenol on BLAC-800.

The intraparticle diffusion model is shown in Fig. S3 and Table S1. For detailed analysis, see supplementary material.

Adsorption isotherms

The equilibrium isothermal adsorption of CSLAC-800, LSAC-800 and BLAC-800 was studied by preparing phenol solutions with initial concentrations of 150, 300, 500, 1000, 1500 and 2000 mg/L, respectively. The fitting results of Langmuir and Freundlich isotherm adsorption models are shown in Fig. 11 and

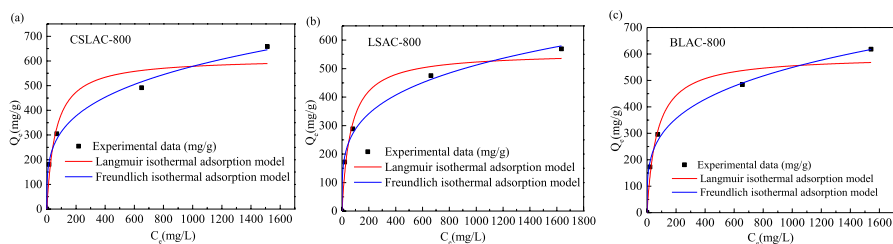


Fig. 11 Fitting curve of isothermal adsorption model for CSLAC-800 (a), LSAC-800 (b) and BLAC-800 (c)

Table 3 Fitting results of isothermal adsorption models of CSLAC-800, LSAC-800 and BLAC-800 adsorbents

Adsorption model	Parameters	CSLAC-800	LSAC-800	BLAC-800
Langmuir isothermal adsorption model	Q_{\max} (mg g ⁻¹)	612.3	556.9	592.7
$Q_e = \frac{Q_{\max} K_L C_e}{1 + K_L C_e}$	K_L	0.0170	0.0154	0.0147
	R^2	0.9337	0.9756	0.9622
Freundlich isothermal adsorption model	$1/n$	0.2658	0.2515	0.2697
$Q_e = K_F C_e^{1/n}$	K_F	92.17	90.19	85.22
	R^2	0.9936	0.9935	0.9947

Table 3. The correlation coefficients R^2 of Langmuir model of CSLAC-800, LSAC-800 and BLAC-800 were 0.9337, 0.9756 and 0.9622, respectively, which were lower than those of Freundlich model (0.9936, 0.9935, 0.9947). Therefore, the Freundlich model can define the adsorption isotherms of phenol on three kinds of lignin-based activated carbon, indicating that the phenol molecules adsorbed on the adsorbent are mainly heterogeneous multi-molecular layers. According to Langmuir isothermal model, the maximum adsorption capacity (Q_m) of phenol was 612 mg/g, 557 mg/g and 593 mg/g, respectively, and Freundlich parameter $1/n$ was between 0.1 and 0.5, indicating that phenol could be easily adsorbed to the adsorbent.

According to Langmuir adsorption isotherm, the maximum adsorption capacity of the three lignin-based activated carbons in this paper was known, and the adsorption capacity of phenol by biomass activated carbons in existing studies was compared, as shown in Table S2. There are few reports on the use of waste lignin to prepare activated carbon for the adsorption of phenol. A large number of studies directly prepare activated carbon from various biomass for the adsorption of phenol. The adsorption capacity of biomass activated carbon for phenol was lower than that of lignin-based activated carbon. Therefore, using waste lignin to prepare activated carbon can effectively treat phenol containing wastewater, to achieve the purpose of waste treatment waste.

Thermodynamic parameters

By changing the temperature of the adsorption system, the thermodynamic parameters of phenol adsorption on three kinds of lignin-based activated carbon were determined, including Gibbs free energy change (ΔG°), enthalpy change (ΔH°) and entropy change (ΔS°). The Gibbs free energy change is expressed as follows:

$$\Delta G^\circ = -RT \ln K_D \quad (7)$$

where R is the gas constant (8.314 J/mol K), T is the absolute temperature (K), and K_D is the distribution constant, which can be calculated by the following equation.

$$K_D = \frac{q_e}{C_e} \times \frac{m}{V} \quad (8)$$

q_e is the adsorption capacity when the adsorbent adsorbs phenol to equilibrium, and C_e is the concentration of phenol when the solution reaches equilibrium. m is the mass of adsorbent (g) and V is the volume of phenol solution (L).

The values of ΔH° and ΔS° can be obtained from Gibbs–Helmholtz equation, and the formula is as follows:

$$\Delta G^\circ = \Delta H^\circ - T\Delta S^\circ \quad (9)$$

Equation (10) is obtained from Eqs. (7) and (9), as shown below:

$$\ln K_D = \frac{\Delta S^\circ}{R} - \frac{\Delta H^\circ}{RT} \quad (10)$$

Therefore, ΔS° (J/mol K) and ΔH° (kJ/mol) are obtained from the intercept and slope of the linear curve of $\ln K_D$ and $1/T$, that is, the entropy change ΔS° is obtained from the intercept, and the enthalpy change ΔH° is obtained from the slope [58, 59].

The thermodynamic calculation results obtained are shown in Table 4, the ΔG° range of the three lignin-based activated carbons is -6.25 kJ/mol to -3.43 kJ/mol, indicating that the adsorption between the adsorbents and phenol is mainly physical adsorption, with a negative value of ΔG° , indicating that the adsorption can be spontaneous within the temperature range. As can be seen from Table 4, ΔH° is -45.62 kJ/mol, -32.55 kJ/mol and -33.49 kJ/mol, respectively, indicating that the adsorption process is exothermic. According to relevant literature, if ΔH° is

Table 4 Thermodynamic parameters of adsorption of phenol by CSLAC-800, LSAC-800 and BLAC-800 adsorbents

Adsorbent	ΔG (KJ/mol)			ΔH (KJ/mol)	ΔS (J/mol K)
	303 (K)	313 (K)	323 (K)		
CSLAC-800	-6.25	-5.25	-3.55	-45.62	-129.57
LSAC-800	-5.29	-3.61	-3.46	-32.55	-90.71
BLAC-800	-5.36	-4.88	-3.43	-33.49	-92.31

less than 40 kJ/mol, physical adsorption controls the adsorption process; if ΔH° is greater than 80 kJ/mol, chemisorption mainly controls the adsorption process; if ΔH° is between 40 kJ/mol and 80 kJ/mol, adsorption may be attributed to physical and chemical adsorption. More thermodynamic parameters are needed to distinguish which factor has the greatest influence on the adsorption process. The adsorption of the three lignin-based activated carbons obtained from ΔH° is mainly physical adsorption, while there are some other interactions, such as π - π interaction and hydrogen bond interaction. ΔS° represents the randomness of the solid-liquid interface. ΔS° is -129.57 J/mol K, -90.71 J/mol K, -92.31 J/mol K, respectively, indicating that the randomness of the solid-liquid interface decreases after the adsorption process [60–63].

Mechanism research

Activation mechanism of lignin activated carbon

Activated carbon was prepared from lignin raw materials. Figure 12 shows the pyrolysis of lignin macromolecules into small molecular fragments under the alkali activator at high temperature. Lignin-based activated carbon contains fragments of lignin structural monomer and various mixed small molecular fragments [64–66].

Adsorption mechanism of phenol on lignin-based activated carbon

Figure 13 shows the adsorption mechanism of phenol on lignin-based activated carbon. The adsorption process is carried out by combination of physical adsorption and chemical adsorption. As shown in Fig. 13, phenol mainly interacted with oxygen-containing functional groups and aromatic ring groups on the surface of activated carbon via hydrogen bond and π - π interaction [16, 67, 68]. The combination of physical adsorption and chemical adsorption improves the adsorption capacity of activated carbon for phenol.

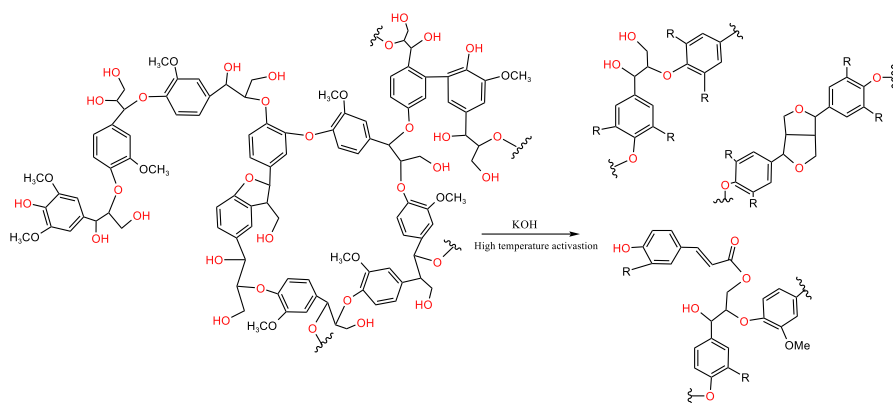
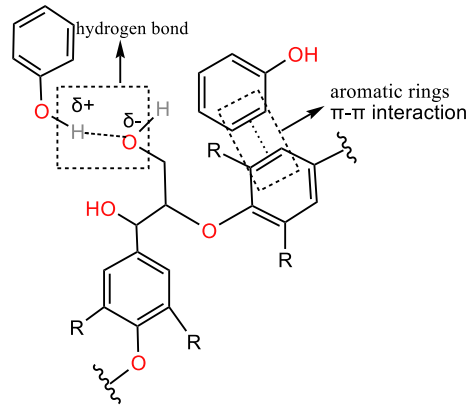


Fig. 12 Decomposition mechanism of lignin macromolecules

Fig. 13 Adsorption mechanism of phenol on lignin-based activated carbon



Conclusions

The different lignin-based biomass activated carbons were prepared by KOH activation from three different lignin sources, and the effects of different lignin sources, activation temperatures and adsorption conditions on the removal of phenol were systematically investigated. The results showed that the specific surface area of CSLAC-800 (1679 m²/g) was much higher than that of LSAC-800 (844 m²/g) and BLAC-800 (856 m²/g) prepared under the same conditions. The effects of three lignin-based activated carbons on the removal rate of phenol under the same modification conditions and adsorption conditions (such as adsorbent dosage, adsorption temperature and pH value) were systematically studied. The results showed that the adsorption rates of the three lignin-based activated carbons were significantly increased after modification compared with those before modification. The adsorption rates of phenol by the three lignin-based activated carbons increased sharply in the first 15 min, then increased slowly and finally reached a stable value. After adsorption for 60 min, the adsorption basically reached equilibrium. The maximum adsorption capacities of CSLAC-800, LSAC-800 and BLAC-800 for phenol in natural phenol solution at 30 °C were 612 mg/g, 557 mg/g and 593 mg/g, respectively. The experimental results show that the adsorption of phenol on CSLAC-800 and BLAC-800 conforms to the pseudo-second-order kinetic model and Freundlich isothermal adsorption model, indicating that heterogeneous multimolecular layer adsorption is dominant. The adsorption of phenol on LSAC-800 accords with pseudo-first-order kinetic model and pseudo-second-order kinetic model and Freundlich isothermal adsorption model. The thermodynamic parameters showed that the three lignin-based activated carbons adsorbed phenol spontaneously and exothermically, and the adsorption is mainly through the π - π and hydrogen bond interactions, and hydrophobic effect.

Supplementary Information The online version contains supplementary material available at <https://doi.org/10.1007/s11164-023-04958-z>.

Authors' contributions ML was involved in experimental research, writing—original draft, formal analysis, validation. JM helped in experimental research. YL contributed to formal analysis. HW was involved in characterization. YW helped in analysis of experimental results. HS contributed to writing review and editing, supervision, project administration, funding acquisition.

Funding This research did not receive any specific grant from funding agencies in the public, commercial or not-for-profit sectors.

Availability of data and materials The datasets generated and/or analyzed in the course of the current study are available from the corresponding author on reasonable request.

Declarations

Competing interests The authors declare no competing interests.

Conflict of interests The authors declare that they have no known competing financial interests or personal relationships that could have appeared to influence the work reported in this paper.

Ethical approval This article does not involve any animal experiment or human subject experiment.

References

1. S. Mishra, S.S. Yadav, S. Rawat, J. Singh, J.R. Koduru, *J. Environ. Manag.* **246**, 362 (2019)
2. X. Peng, K. Zheng, J. Liu, Y. Fan, C. Tang, S. Xiong, *Environ. Toxicol. Chem.* **37**, 7 (2018)
3. W.Y. Du, Y. Xiao, J.J. Yao, Z. Hao, Y.B. Zhao, *Exp. Ther. Med.* **13**, 1 (2017)
4. W. Duan, F. Meng, H. Cui, Y. Lin, G. Wang, J. Wu, *Ecotox. Environ. Safe* **157**, 441 (2018)
5. Z. Darvishi Chaghaganoj, N. Asasian-Kolur, S. Sharifian, M. Sillanpää, *J. Environ. Chem. Eng.* **9**, 4 (2021)
6. Z. Dong, R. Zhou, L. Xiong, H. Li, Q. Liu, L. Zheng, Z. Guo, *Z. Deng Nanoscale Adv.* **2**, 1 (2020)
7. Q. Sun, M. Liu, K. Li, Y. Zuo, Y. Han, J. Wang, C. Song, G. Zhang, X. Guo, *CrystEngComm* **17**, 37 (2015)
8. J.L. Jing Shen, F. Li, H. Zhao, Z. Dua, F. Cheng, *Chem. Eng. J.* **417**, 128091 (2020)
9. A.K. Singh, M. Bilal, H.M.N. Iqbal, A.S. Meyer, A. Raj, *Sci. Total Environ.* **777**, 145988 (2021)
10. L. Liu, S.J. Tan, T. Horikawa, D.D. Do, D. Nicholson, J. Liu, *Adv. Colloid Interface* **250**, 64 (2017)
11. K. Jun, Han, Yoon. Kim and Park *WATER-SUI* **11**, 9 (2019)
12. G. Issabayeva, S.Y. Hang, M.C. Wong, M.K. Aroua, *Rev. Chem. Eng.* **34**, 6 (2018)
13. A. Ahmad, S. Hamidah Mohd Setapar, A. Ali Yaqoob, M. Nasir Mohamad Ibrahim, *Mater Today: Proceedings* **47**, 1359 (2021)
14. Z. Chai, P. Lv, Y. Bai, J. Wang, X. Song, W. Su, G. Yu, *RSC Adv.* **12**, 11 (2022)
15. N.A. Khan, S.H. Jhung, *J Hazard Mater* **325**, 198 (2017)
16. A. Supong, P.C. Bhomick, R. Karmaker, S.L. Ezung, L. Jamir, U.B. Sinha, D. Sinha, *Appl Surf Sci* **529**, 147046 (2020)
17. R. Singh, R.K. Dutta, D.V. Naik, A. Ray and P.K. Kanaujia, *Environ. Chall* **5**, 100353 (2021)
18. I. Stoycheva, B. Tsyntsarski, B. Petrova, G. Georgiev, T. Budinova, N. Petrov, B. Trzebiecka, S. Pusz, B. Kumanek, U. Szeluga, *Appl. Sci.* **12**, 4 (2022)
19. D.S.P. Franco, J. Georgin, M.S. Netto, D. Allasia, M.L.S. Oliveira, E.L. Foletto, G.L. Dotto, *J. Environ. Chem. Eng.* **9**, 5 (2021)
20. T. Song, R. Deng, J. Gao, J. Yi, P. Liu, X. Yang, Z. Zhang, B. Han, Y. Zhang, *Ind. Crop. Prod.* **180**, 114764 (2022)
21. D. Stewart, *Ind Crop Prod* **27**, 2 (2008)
22. D. Kai, M.J. Tan, P.L. Chee, Y.K. Chua, Y.L. Yap, X.J. Loh, *Green Chem* **18**, 5 (2016)
23. M. Lievonon, J.J. Valle-Delgado, M.-L. Mattinen, E.-L. Hult, K. Lintinen, M.A. Kostianen, A. Paananen, G.R. Szilvay, H. Setälä, M. Österberg, *Green Chem.* **18**, 5 (2016)

24. S.I. Mussatto, M. Fernandes, G.J. Rocha, J.J. Orfao, J.A. Teixeira, I.C. Roberto, *Bioresource Technol* **101**, 7 (2010)
25. K. Fu, Q. Yue, B. Gao, Y. Sun, L. Zhu, *Chem. Eng. J.* **228**, 1074 (2013)
26. Y. Gao, Q. Yue, B. Gao, Y. Sun, W. Wang, Q. Li and Y. Wang, *Chem. Eng. J.* **217**, 345 (2013)
27. J.-P. Simonin, *Chem. Eng. J.* **300**, 254 (2016)
28. N. Ponomarev, O. Pastushok, E. Repo, B. Doshi, M. Sillanpää, *A.C.S. Appl. Nano Mater.* **2**, 9 (2019)
29. E.C. Nnadozie, P.A. Ajibade, *Data Brief* **32**, 106292 (2020)
30. A. Arabpour, S. Dan, H. Hashemipour, *Arab. J. Chem.* **14**, 3 (2021)
31. L.N. Rozanov, *Vacuum* **189**, 110267 (2021)
32. P. Mishra, K. Singh and U. Dixit, *Sustain. Chem. Pharm.* **22**, 100491 (2021)
33. C. Vasile, G.E. Zaikov, *New trends in natural and synthetic polymer science* (Nova Publishers, Hauppauge, 2006)
34. C. Liu, J. Hu, H. Zhang, R. Xiao, *Fuel* **182**, 864 (2016)
35. T. Nakamura, H. Kawamoto, S. Saka, *J. Anal. Appl. Pyrol.* **81**, 2 (2008)
36. J. Kibet, L. Khachatryan, B. Dellinger, *Environ. Sci. Technol.* **46**, 23 (2012)
37. S. Hu, Y.-L. Hsieh, *J. Mater. Chem. A* **1**, 37 (2013)
38. J. Liu, Y. Liu, J. Peng, Z. Liu, Y. Jiang, M. Meng, W. Zhang, L. Ni, *Water Air Soil Poll.* **229**, 12 (2018)
39. T.C.E. Gonzalez-Serrano, J. Rodríguez-Mirasol, J. Rodríguez, *Mater. Interfaces* **36**, 11 (1997)
40. Y. Wang, S.L. Wang, T. Xie, J. Cao, *Bioresource Technol.* **316**, 123929 (2020)
41. J. Zhou, A. Luo, Y. Zhao, *J. Air Waste Manag.* **68**, 12 (2018)
42. Z. Xu, Z. Yuan, D. Zhang, W. Chen, Y. Huang, T. Zhang, D. Tian, H. Deng, Y. Zhou and Z. Sun, *J. Clean Prod.* **192**, 453 (2018)
43. M. Jain, S.A. Khan, A. Sahoo, P. Dubey, K.K. Pant, Z.M. Ziora, M.A.T. Blaskovich, *Bioresource Technol.* **352**, 127030 (2022)
44. S. Lv, C. Li, J. Mi, H. Meng, *Appl Surface Sci.* **510**, 145425 (2020)
45. K.C. Bedin, A.C. Martins, A.L. Cazetta, O. Pezoti, V.C. Almeida, *Chem. Eng. J.* **286**, 476 (2016)
46. W. Jin, D. Shen, Q. Liu, R. Xiao, *Polym. Degrad. Stab.* **133**, 65 (2016)
47. S. Wang, H. Lin, B. Ru, W. Sun, Y. Wang, Z. Luo, *J. Anal. Appl. Pyrol.* **108**, 78 (2014)
48. M.A. Bedmohata, A.R. Chaudhari, S.P. Singh, M.D. Choudhary, *Int. J. Adv. Res. Chem. Sci.* **2**, 8 (2015)
49. M. Kumar, S.N. Upadhyay, P.K. Mishra, *Bioresource Technol. Rep.* **8**, 100186 (2019)
50. S.A. Sajjadi, A. Mohammadzadeh, H.N. Tran, I. Anastopoulos, G.L. Dotto, Z.R. Lopicic, S. Sivamani, A. Rahmani-Sani, A. Ivanets, A. Hosseini-Bandegharai, *J. Environ. Manag.* **223**, 1001 (2018)
51. S. Xia, N. Cai, J. Wu, H. Xiao, J. Hu, X. Chen, Y. Chen, H. Yang, X. Wang, H. Chen, *Fuel Process Technol.* **209**, 106543 (2020)
52. F. Ghorbani, S. Kamari, S. Zamani, S. Akbari, M. Salehi, *Surface Interfaces* **18**, 100444 (2020)
53. M.A.A. Akl, *J. Anal. Bioanal. Tech.* **5**, 2 (2014)
54. G. Lv, J. Liu, Z. Xiong, Z. Zhang, Z. Guan, *J. Chem. Eng. Data* **61**, 11 (2016)
55. L. Jiang, Y. Chen, Y. Wang, J. Lv, P. Dai, J. Zhang, Y. Huang, W. Lv, *ACS Omega* **7**, 12 (2022)
56. F. Tomul, Y. Arslan, B. Kabak, D. Trak, H.N. Tran, *J. Chem. Technol. Biot.* **96**, 4 (2021)
57. M. Li, Y. Wang, Y. Liu, H. Wang, H. Song, *Res. Chem. Intermediat.* **48**, 4 (2022)
58. M. Zbair, K. Ainassaari, A. Drif, S. Ojala, M. Bottlinger, M. Pirila, R.L. Keiski, M. Bensitel, R. Brahma, *Environ. Sci. Pollut. Res. Int.* **25**, 2 (2018)
59. E.C. Lima, A. Hosseini-Bandegharai, J.C. Moreno-Piraján, I. Anastopoulos, *J. Mol. Liquids* **273**, 425 (2019)
60. N.A.S. Mohammed, R.A. Abu-Zurayk, I. Hamadneh, A.H. Al-Dujaili, *J. Environ. Manag.* **226**, 337 (2018)
61. T. Phatthanakitiphong, G. Seo, *Nanomater. Basel* **6**, 7 (2016)
62. L. Spessato, K.C. Bedin, A.L. Cazetta, I. Souza, V.A. Duarte, L.H.S. Crespo, M.C. Silva, R.M. Pontes, V.C. Almeida, *J. Hazard Mater.* **371**, 499 (2019)
63. N. Douara, B. Bestani, N. Benderdouche, L. Duclaux, *Desalin Water Treatm.* **57**, 12 (2015)
64. A. Agarwal, M. Rana, J.-H. Park, *Fuel Process Technol.* **181**, 115 (2018)
65. C. Chio, M. Sain, W. Qin, *Renew. Sustain. Energ. Rev.* **107**, 232 (2019)
66. B. Wang, S.-F. Wang, S.S. Lam, C. Sonne, T.-Q. Yuan, G.-Y. Song, R.-C. Sun, *Renew. Sustain. Energ. Rev.* **134**, 110384 (2020)
67. X. Kong, H. Gao, X. Song, Y. Deng, Y. Zhang, *Chem. Phys. Lett.* **739**, 137046 (2020)

68. T.V. Tran, V.D. Cao, V.H. Nguyen, B.N. Hoang, D.-V.N. Vo, T.D. Nguyen, L.G. Bach, J. Environ. Chem. Eng. **8**, 1 (2020)

Publisher's Note Springer Nature remains neutral with regard to jurisdictional claims in published maps and institutional affiliations.

Springer Nature or its licensor (e.g. a society or other partner) holds exclusive rights to this article under a publishing agreement with the author(s) or other rightsholder(s); author self-archiving of the accepted manuscript version of this article is solely governed by the terms of such publishing agreement and applicable law.